Ciencia Nicolaita 95: 1-14; Diciembre de 2025 doi:10.35830/cn.vi95.875

Indirect estimates of scalar-tensor modifications of the growth of structure at large scales

Ana Avilez López[1,2]

[1] Facultad de Ciencias Físico Matemáticas, Benemérita Universidad Autónoma de Puebla, Av. San Claudio SN, Col. San Manuel, Puebla, México.
[2] Centro Internacional de Física Fundamental, Benemérita Universidad Autónoma de Puebla, Apdo. Postal 1152, Puebla, Pue., México

Dates
Received: July 2nd, 2025
Accepted: November 5th, 2025
Available online: December 2025

Corresponding author
Ana Avilez-López
email: ana.avilezlopez@correo.buap.mx

Abstract

An estimate to possible modifications to the growth of structure at very large scales according to cosmological observations different to direct measurements of LSS is derived. In order to do so, we construct and constrain the Effective Scalar-Tensor theory (EST) which arises as a phenomenological setup for modified theories of gravity as a first approximation in the very large scales limit where non-linearities are negligible. Estimates of the EST parameters are made using observations of the CMB from Planck and WMAP9(pol), along with other complementary data which lead to an indirect determination of the growth rate of LSS. It is assumed that the growth behaves as a general power law $\mu = \mu_0(1 + ra^s)$ which is one-to-one mapped to an specific effective scalar-tensor theory defined by $\omega(a) = m\, a^n$ where $m = 1/2r\mu_0$ and $n = -s$. We derive a 1σ constraint for the exponent $n = -0.47^{+0.32}_{-0.47}$ and $m = 50.1 \pm 11.2$ or $m > 3.2 \times 10^3$ according to measurements of the CMB anisotropies from Planck and complementary data from BAO and HST. The result suggests two possible regimes where modifications of the growth may be detected in redshift surveys: 1) $\frac{\mu}{\mu_0} - 1 < 6.2 \times 10^{-3} a^{0.47^{-0.32}_{+0.47}}$ and 2) $\frac{\mu}{\mu_0} - 1 = 10^{-2} \pm 0.089 \times a^{0.47^{-0.32}_{+0.47}}$.

Keywords: Cosmology, Scalar-Tensor Theories, Large Scale Structure of the Universe

Introduction

The large-scale structure of the universe is expected to be observed with unprecedent accuracy by the next generation surveys. These observations will provide a whealthy source of data to probe the relationship between matter overdensities and the geometry of space-time quantified by the gravitational potentials. Any metric theory of gravity predicts a specific form for this reltionship. These predictions for alternative theories of gravity depart from those of the standard model based on General Relativity. Therefore, this upcoming data will allow us to estimate the viability of a variety of theoretical prescriptions of gravity inlcuding the standard model.

A usual way to handle these generic modifications of the growth of structure within linear perturbation theory is to parametrize the standard equations describing the dynamics of sub-horizon perturbations in the Newtonian-Conformal gauge in the quasi-static limit. As explained in (Song et al., 2010; L. Pogosian & Zhao, 2010; Hojjati et al., 2012), such parameterizing functions are related to the growth of structure and other observable quantities. If we were able to measure them at every scale and redshift, we would determine a specific theoretical model to describe LSS inhomogeneities. However, such task is difficult if not impossible so far. A more feasible option would be to reduce the space of models by taking a wide set of parametric models based in a particular modified theory. Therefore, the huge task determining two free functions is reduced to estimate parameters. Within the context of models where gravity is modified at large scales aiming to predict the ex-

pansion of the universe, a general phenomenological setup has been proposed by Song et al. (Song et al., 2010). In that work they consider models in which the modification of gravity is achieved by a scalar field coupled to the metric. They assume a massless scalar and they neglect self interactions at linear scales since they only play the role of screening the scalar at small scales, though they may still have considerable effect at large scales this only happens due to non-linear effects. At the end they get the set of Bergmann-Wagoner scalar-tensor theories (Bergmann, 1968). The starting point of this work is indeed such phenomenological setup, an extra simplification we make is to consider a power-law functional form of the growth, the reason of doing this is that its form in the standard model behaves as a very specific power law given by $\Omega_m^{0.6}$ (Dodelson, 2003; Peebles, 1993), so that it is reasonable to consider a generic power-law. What we get at the end is a particular form for the theory free function $\omega(\phi(a))$ given by a power law of the scale factor as well. We dub such particular subset of the Bergmann-Wagoner scalar-tensor theories the effective scalar-tensor theories (EST). Thus, we identify a one-to-one mapping since any specific form of the growth corresponds to a specific function $\omega(\phi(a))$ which uniquely defines a particular EST. This correspondence between the growth and the parameters of gBDT is very useful since it allows us to indirectly derive constraints to growth by using constraints of the parameters of EST and viceversa.

The main goal of this work is to derive an estimate for possible modifications of the growth by using estimations of the parameters of EST by using cosmological observations different to direct observations of LSS. We study the cosmological theoretical predictions of EST in order to figure out observational signatures leading to test the theory with sensible data. We sample the parameter space of EST in order to compute the likelihood function corresponding to recent CMB observations from Planck and other complementary data. This allows us to estimate the range of values of the EST parameters allowed by recent observations and hence to derive indirectly a bound for possible modifications of the growth allowed by these datasets.

This paper is organized as follows, in section 2 we review the construction of EST from the phnomenological setup first proposed by (Song et al., 2010). In section 3 we study the EST model for a perturbed flat FRW universe with standard ΛCDM matter-energy content. We analyse some cosmological predictions either from the background evolution and for perturbations in order to figure out qualitatively the extent of sensitivity of the observables to the parameters aiming to single out possible detectable effects. In section 4 we present methodology and technical aspects of the bayesian analysis we carried out. In the fifth section we present and discuss the results. Finally, we make our conclusions at section 6.

2. A Phenomenological Setup for Modified Gravity

In order to understand the evolution of inhomogeneities at small scales it suffices to study the dynamics of sub-horizon perturbations in the quasi-static limit which is fully described by the Newtonian prescription. In order to describe the geometry of this perturbed universe we use the perturbed Friedmann-Robertson-Walker metric in the Newtonian-Conformal gauge

$$ds^2 = -(1+2\Psi)dt^2 + a(t)^2(1+2\Phi)\delta_{ij}dx^i dx^j, \quad (1)$$

where Φ and Ψ correspond to the gauge invariant Bardeen potentials which represent the gravitational potential in the Newtonian limit. The scale factor $a(t)$ quantifies the expansion of the universe. In order to take into account possible modifications to the growth of sub-horizon perturbations usually some undetermined functions η and Q are introduced as follows [1]

$$\begin{aligned} k^2\Phi &= 4\pi G_N a^2 Q(a,k)\rho_m\Delta_m, \\ \Phi &+ \eta\Psi = 0, \end{aligned} \quad (2)$$

$\eta(a,k)$ and $Q(a,k)$ are free functions of the scale factor and the wavenumber and are directly related to observable quantities at different epochs and scales. On one hand, measurements of the Newtonian potential Φ (and then Q) can be obtained directly from galaxy distribution, however this is difficult due to the bias of galaxies. On the other

[1] if no anisotropic stress at late times is assumed to exist.

hand, weak lensing and Integrated-Sachs-Wolfe (ISW) effect are sensitive to $\frac{\Phi-\Psi}{2} \sim \frac{Q}{2}(1+\eta^{-1})$ which is an unbiased quantity. Additionally, peculiar velocities are proportional to $\Psi \sim \frac{Q}{\eta}$. In principle, Q, Σ and η might be constrained in a model-independent way, however a quite large number of degrees of freedom are to be determined with a very small amount of observational data. So we are forced to abandon the fully model-independent approach and instead we can use a wide set of parametric models. Regarding to physically viable theories in which a modification of gravity is accomplished by an scalar degree of freedom $\phi = \bar{\phi} + \delta\phi$, the Hordenski theory (HT) represents a large class of this kind. Because we are focusing on the linear regime, it is reasonable to to pick the subset of HT whose perturbation $\delta\phi$ tend to that within the Brans-Dicke theory at large scales, as prescribed by the reduced Horndeski theories (RHT) proposed at (Avilez & Skordis, 2014).

In first place, it is well known that, at the level of the background, there exists a degeneracy between ΛCDM and other models like DGP, Galileons, etc. since all of them predict considerably well the observed expansion of the universe. Thus a different kind of phenomena is needed to break down this degeneracy. For instance, observations of the dynamics of coherent sub-horizon linear perturbations. In the limit mentioned above, the equations for the HBDT describing their dynamics reduce to

$$\begin{aligned} \Phi - \Psi &= \delta\phi, \\ k^2\Phi &= 4\pi G_N a^2 \rho_m \delta_m + \frac{k^2}{2}\delta\phi, \\ (2\omega+3)k^2\delta\phi &= -8\pi G_N a^2 \rho_m \delta_m - \mathcal{I}(\delta\phi), \end{aligned} \quad (3)$$

where ω corresponds to the Brans-Dicke parameter, ρ_m and δ_m are the matter background density and the density contrast of matter respectively, with

$$\begin{aligned} \mathcal{I}(\delta\phi) &= M^2\delta\phi + \int \frac{d^3k_1 d^3k_2}{(2\pi)^2}\delta(k-(k_1+k_2)) \\ &\times \; M(k_1,k_2)\delta\phi(k_1)\delta\phi(k_2). \end{aligned}$$

The M parameter controls the extent of self-interaction of the scalar degree of freedom of gravity. These interactions are important only at the non-linear regime at very small scales, however they are not relevant for linear cosmological perturbations. It is important to point out that effectively G_N and ω can be functions of the scale factor.

From the previous equations we can obtain analytically η and Q

$$\begin{aligned} Q(k,a) &= \frac{2+2\omega+M^2a^2/k^2}{3+2\omega+M^2a^2/k^2}, \\ \eta(k,a) &= \frac{2+2\omega+M^2a^2/k^2}{4+2\omega+M^2a^2/k^2}, \\ \mu(k,a) &= \frac{Q}{\eta}. \end{aligned}$$

Though it sounds obvious, we want to state clear that the parameterizing functions reduce to one in the case of GR. For EST there are two ways to recover GR : $\omega \gg 1$ or $\frac{M^2a^2}{k^2} \gg 1$. From the previous equations we can notice that because $\Sigma = 1$ either the ISW effect and the lensing potential remain the same as in GR.

On one hand, it is a well known result in GR that $\mu_0 \sim \Omega_m^{0.55}$ (Dodelson, 2003; Peebles, 1993). On the other hand we only expect small deviations from the GR predictions within EST, as we already mentioned it is quite reasonable to assume that overdensities grow as in GR plus a small modification behaving as a power law of the scale factor as well

$$\mu = \mu_0(1 + ra^s). \quad (4)$$

For coherent perturbations the linear M^2 term may be important, however because it has been strongly constrained in (Faraoni, 2009) we assume $M^2 \sim 0$. By combining equations (3), the difference of the Bardeen potentials can be written in terms of the density contrast of matter and the Brans-Dicke parameter such that the power law ansatz for μ can be related to an specific power law of ω given by

$$\omega(a) + \frac{3}{2} = \frac{1}{2r\mu_0 a^s} = ma^n \quad (5)$$

where $m = 1/2r\mu_0$ and $n = -s$. Such functional form arises. Thus, for every specific modification of the growth there is a unique scalar-tensor theory defined by (5)

In this work we go beyond the quasi-static limit. Our goal in this work is to test the growth indirectly by estimating the parameters of EST for a full range of scales and hence we take into account relativistic effects. Therefore, care should be taken about the implications mentioned above. For instance, since μ parametrizes the linear growth, it can also be interpreted alternatively as a classical "running" G_N constant in the quasi-static limit. However, beyond that limit, the Newton constant is much more than that, and even in the simplest cases like BDT and EST such interpretation of the growth is not valid. Actually the dynamical G_N encodes much richer phenomenology beyond the growth. Furthermore, in more complicated frameworks such as the Horndeski-like theories, screening mechanisms arise naturally and the GR predictions at small scales are recovered, in turn, at cosmological scales the extra degrees of freedom show up and G_N affects not only the growth but the whole set of cosmological predictions. Indeed, in the specific case of EST the scalar itself plays the role of such dynamical coupling.

3. The Model

The action describing the general scalar-tensor theories is given by

$$S = \frac{1}{16\pi G_N}\int d^4x\sqrt{-g}\left[\phi R - 2\Lambda - \frac{\omega(\phi)}{\phi}(\nabla\phi)^2\right] + S_m,$$

where matter couples minimally to the metric and the scalar affects matter only indirectly by means of the metric, so the evolution of matter is determined by the conservation equations. The local value of the scalar field is related to the Newton constant that we measure in a Cavendish-like experiments in order to implement the Mach principle.

Let us consider a universe with flat, homogeneous and isotropic spacetime and ΛCDM matter-energy content. The modified Einstein equations describing the geometry of this universe within EST reduce to a modified version of the usual Friedmann and Raychaudhury equations given by (Dodelson, 2003)

$$\left(H + \frac{1}{2}\frac{\dot{\bar{\phi}}}{\bar{\phi}}\right)^2 = \frac{8\pi G_N}{\bar{\phi}}\rho + \frac{\Lambda}{\bar{\phi}} + f(\omega)\left(\frac{\dot{\bar{\phi}}}{\bar{\phi}}\right)^2$$

$$-2\dot{H} - 3H^2 - \frac{\ddot{\bar{\phi}}}{\bar{\phi}} - 2H\frac{\dot{\bar{\phi}}}{\bar{\phi}} - \frac{\omega}{2}\left(\frac{\dot{\bar{\phi}}}{\bar{\phi}}\right)^2 = \frac{8\pi G_N}{\bar{\phi}}P - \frac{\Lambda}{\bar{\phi}}.$$

The evolution of the background scalar $\bar{\phi}$ in a flat FRW universe is governed by

$$\ddot{\bar{\phi}} + 3H\dot{\bar{\phi}} = \frac{1}{2\omega+3}\left[8\pi G_N(\rho - 3P) + 4\Lambda - \frac{d\omega}{d\bar{\phi}}(\dot{\bar{\phi}})^2\right],$$

where $\dot{\bar{\phi}} = \frac{d\bar{\phi}}{dt}$ and $H = \frac{\dot{a}}{a}$ with t the proper time.

In the particular case we are concerned of, $\frac{d\omega}{d\bar{\phi}} = \frac{Ha}{\dot{\bar{\phi}}}\frac{d\omega}{da} = \frac{Ha}{\dot{\bar{\phi}}}\, nm\, a^{n-1}$. For $n = 0$ we clearly have the original Brans-Dicke theory.

Strictly speaking, the initial conditions must be fixed by the boundary conditions of the solution on small scales where observers in bound systems in the quasi-static regime like our solar system, would measure (Brans & Dicke, 1961; Clifton, Ferreira, Padilla, & Skordis, 2012)

$$\bar{\phi}_0 = \frac{1}{G_N}\frac{4+2\omega_0}{3+2\omega_0},$$

where $\omega_0 = \omega(a=1) = m$.

We use units where $\bar{\phi}_0$ is dimensionless. However, we consider modifications of GR at the very large scales, where $\bar{\phi}_0$ should be allowed to have different values than those for EST, for that reason we study models in which it is a free derived parameter. From now on, we shall call such models as "unrestricted models" (uEST). For completeness, we also consider models which gravitational coupling is fixed as usual, we call them "restricted models" (rEST).

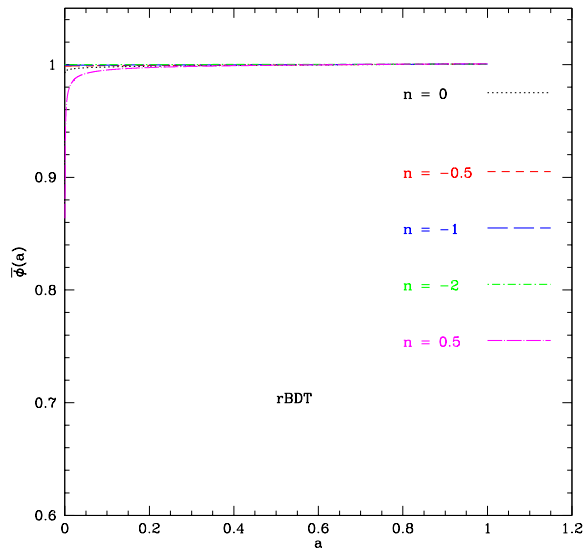

Figure 1. The scalar field solutions for $\omega(a) = ma^n$. As m increases the variation of the field decreases, it determines the value of the gravitational current strength. Negative values of the exponent suppress the scalar while positive ones enhance it.

In contrast to BDT where the field stays approximately constant during the radiation era, EST with $n \neq 0$ might lead to a dynamic solution. Although, during radiation domination the field might hold a non trivial solution since it obeys the following equation

$$\frac{d(a^3\dot{\bar{\phi}})}{da} + \frac{nm\, a^{(n-1)}}{2\omega + 3}(a^3\dot{\bar{\phi}}) = 0.$$

For $n \neq 0$, the solution for the first derivative of the scalar is

$$\dot{\bar{\phi}} \sim a^{-\left(3+\frac{n}{2}\right)}. \tag{6}$$

Notice that $\dot{\bar{\phi}}$ appears in the right hand side of the Friedmann equation, so it can be thought that it plays the role of an extra component of the matter-energy density. If the exponent is negative as $a \to 0$ the field variation tends to infinity. In particular, for theories near to the BDT when limit $n \to 0$ the derivative of the scalar behaves as a matter term density, for larger $n \sim 2$ it behaves the radiation density does. For larger positive values of n $\bar{\phi}'$ would be dominant at early times, however for such large values of $|n|$ the theory is not physically feasible at late times so those effects at early times are not going to be considered.

Figure 1 shows us numerical solution for the scalar over the whole history of the universe within restricted models. Clearly, the trend of the field is the same for a wide range of n values, it grows monotonically along with time. The overall variation of the field is larger as n increases. In order to illustrate better how the field grows at late times, we will use an approximation of (6) for low redshifts $z \ll 1$. In that case $\omega(z) = m(1 - nz)$ and the scalar equation (6) is

$$\left(4 - mn\frac{1}{(2m+3)\phi_0^{-2}}(1 + \frac{2nz}{2m+3})\right) H\dot{\bar{\phi}} = \frac{8\pi G}{2m+3}\Omega_m\left(1 + \frac{3(2m+3)+2n}{2m+3}z\right).$$

Since $z \sim 0$, the approximation works only if we set $\frac{1}{z} \gg |n|$ so that the last term in the r.h.s is small. Within this bounds if $|n| \gg 1$ and $m \sim 1$, then the first term in the left hand side can be neglected and then $\dot{\bar{\phi}}_{z=0} \simeq -\frac{\Omega_m \phi_0^2(m)}{m}\frac{H_0}{n}$. If $n < 0$ the field's variation increases at late times and vice versa for $n > 0$. Since the field evolves monotonically, and its derivative is suppressed by n, then this parameter also suppresses the field, as shown in the figure. It is clear that for large fixed values of m, negative n suppresses more efficiently the scalar. Thus we can expect these two parameters to be strongly correlated. In summary, at the level of the background, at a given small redshift z the GR limit is accomplished at least in two ways: $(m > 1, -\frac{1}{z} \sim n << 0)$ or $(m \to \infty, n = 0)$.

In order to analyse the expansion, consider $m, |n| > 1$ and ignore the radiation term. As $\frac{\dot{\bar{\phi}}}{\bar{\phi}} \sim \frac{H_0}{nm}$ at late time the left hand side correction term FRW is $O(\frac{1}{nm})$ whilst the additional term in the right hand side can be neglected. However, the dominant contribution of m and n comes up from the normalization on G_N in the matter term at the right hand side. For rEST models, the larger the mean value of ω is, the closer is universe to a FRW ΛCDM. As the scalar and its derivative are enhanced when $\omega \to 1$, the universe expands quicker due to the scalar's derivative contribution in the l.h.s of the Friedmann equation. In this models the mean value of G_N has a significant variation for small values of ω whilst it stays constant in the unrestricted case. Thus, in unrestricted models the

effects of $\bar{\phi}$ and $\dot{\bar{\phi}}$ over the expansion are uncoupled since ω and ξ control each of them independently.

In order to understand effects arising from the physics of recombination we shall see how effectively the n parameter affects the visibility function, which is usually interpreted as the probability that a photon interacts with baryons by Compton scattering during recombination. This function is sensitive to the expansion history of the universe which is affected by the dynamics of the gravitational scalar degree of freedom. Let us consider two regimes for both parameters of the model:

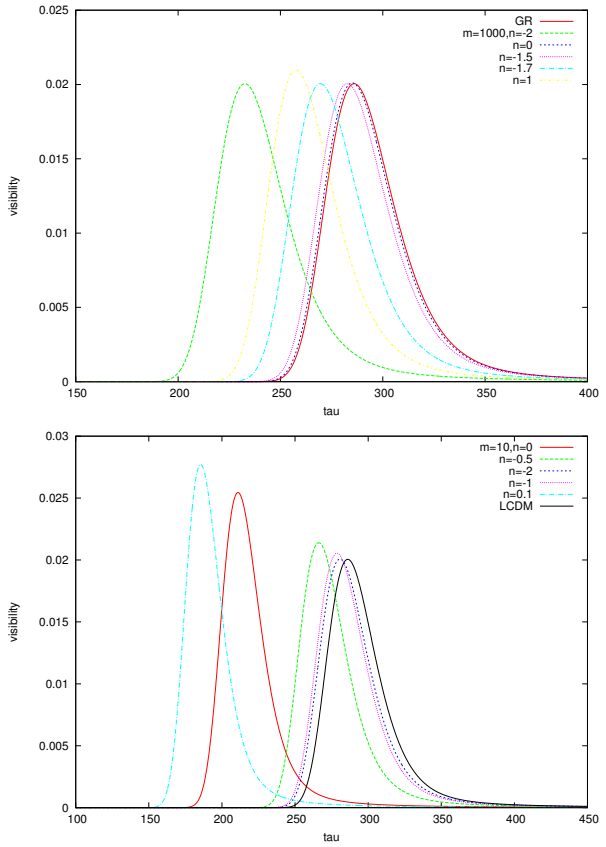

Figure 2. Visibility function for EST in two scenarios: $m = 10$ and $m \to \infty$ and different values of n.

1. $m = 1000$. For large m the model is close to $LCDM$ today and then it is a viable model, if $n < 0$ the whole ω is large all along the expansion history and the visibility approaches to that of GR. Otherwise, when $n > 0$, the scalar is enhanced all along and so the expansion history is greatly modified unless ω is sufficiently large to counter the effect. As shown in **Figure 2**, the width and height of the visibility remains the same for negative values of the exponent. The shift in τ_{rec} happens due to changes in the expansion rate since the temperature $\sim 1eV$ is reached at different time.

2. $m \sim 1$. In this case, unless the exponent is negative and large, the scalar field's effects are important. As in the previous case, increasing the absolute value of the exponent affects the visibility in the same way as in **Figure 2**, as expected the exponent only helps to approach the ΛCDM. It's worth to mention that for $n > 0$ even for small values of n the visibility departs in great extent from ΛCDM then, as we confirm later, they are very likely to be rejected by data as preferred models.

It is important to point out that restricted and unrestricted models with $\phi_0 = 1$ and $n < 0$ tend to be indistinguishable for large values of m as shown in **Figure 3**. On the contrary, even for small values of positive n the visibility of both types of models differs significantly. The reason why this happens is that the expansion rate quickly goes to ΛCDM as $n \to -1$ for a given m. Additionally, regarding the rEST models, since the overall value of ω gets large if $n < 0$, the rescaling factor $(2\omega + 4)/(2\omega + 3)$ of the Newton constant tends to be equal to 1. Otherwise, if $n > 0$ then $(2\omega + 4)/(2\omega + 3) > 1$, the expansion rate is proportional to the gravity strength, so in this case, the rEST model, having weaker Newton's constant than uEST, reaches the time of recombination before and it is easier for electrons to recombine hence the visibility function is slightly narrower than in uEST. We would like to make a comment here regarding matter perturbations in this kind of models, because we have ignored the self-interactions of the scalar, the perturbations are coherent. Thus the growth of sub-horizon matter perturbations only depends non the background evolution. As we are in the Jordan conformal frame the equations for matter perturbations are the same than GR, however the background is not FRW necessarily in this theories, then the matter perturbations grow differently in these models. As mentioned before, in practice EST models are indistinguishable by looking at their expansion history, however thanks to the sensitivity of the growth of matter perturbations to the EST parameters such degeneracy could be broken down. **Figure 4** shows the growth for some models for which the expansion history is practically FRW and the growth of mat-

ter perturbations is modified though. Therefore it would be interesting to test EST by using this sort of measurements.

Another useful tool to probe EST models is the Alcock-Pazcynski test. Although it does not bring important insight when applied to BDT, this effect is sensitive to the n parameter The Alcock-Paczynski effect arises as a consequence of the peculiar velocities of galaxies. Spherical objects i.e. those possessing equal co-moving tangential and radial sizes L_0, appear distorted in the redshift space (Alcock C., 1979). The observed tangential dimension is the angular projection given by

$$\Delta\theta = \frac{L_0}{(z+1)D_A(z)}. \tag{7}$$

The observed radial dimension is given by the redshift projection

$$\delta z = L_0 H(z). \tag{8}$$

There is no need to know L_0 in order to make the measurement since the observable is given by

$$\frac{\Delta z}{\Delta\theta} = (1+z)D_A(z)H(z), \tag{9}$$

this measurement is independent of any assumption about spatial curvature. An Alcock-Paczynski measurement does not necessarily need to be applied to cosmological "objects" but is equally valid for an isotropic process such as the 2-point statistics of galaxy clustering (Ballinger W.E., 1996) (Matsubara T., 1996).

Actually, general analysis of the tangential/radial galaxy clustering pattern in the presence of baryon acoustic oscillations demonstrates how the information may be divided into an overall scale distortion, quantified by a distance parameter (D_A/H), and a warping, quantified by the Alcock-Paczynski distortion factor $D_A H$, enabling the disentangling of D_A and H (Padmanabhan N., 2008) (Taruya A., 2011). Such approaches are just becoming possible with the current generation of large-scale galaxy surveys, and will be very powerful when applied to future datasets such as the Baryon Oscillation Spectroscopic Survey (BOSS) (Eisenstein et al., n.d.).

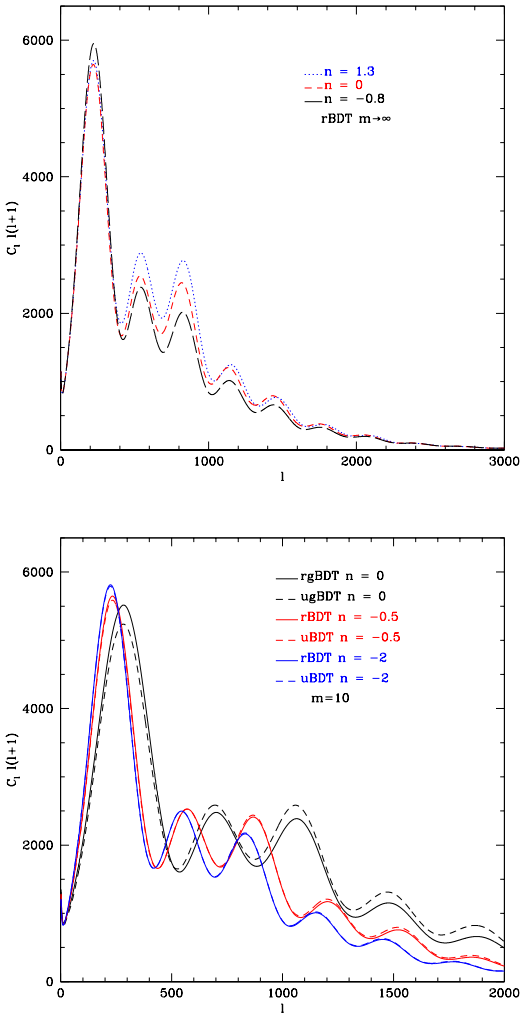

Figure 3. Top: Temperature spectrum in the limit $m \to \infty$ for extreme values of n within the restricted model. Bottom: Restricted an unrestricted ST models are contrasted for small $m(=10)$ and a range of values of n.

As the bottom panel of **Figure 4** shows, the APD for in EST starts to be more sensitive to n from $z > 1$ onwards. As expected such sensitivity is reduced as m increases. As mentioned in previous chapters, $m \to 0$ may be associated with self-accelerating theories when a potential $V(\phi)$ plays the role of dark energy, thus if it is true that our $m \sim 0$ model is an approximation for a shallow-potential case, we can imply that the APD is a powerful test for these self-accelerating theories, such like DGP in the decoupling limit and some $F(R)$.

Anisotropies in the Cosmic Microwave Background

In this subsection we aim to figure out signatures of the EST parameters in the anisotropies of the CMB, that would help us figure out the power of the current measurements to constrain the full set of parameters of EST.

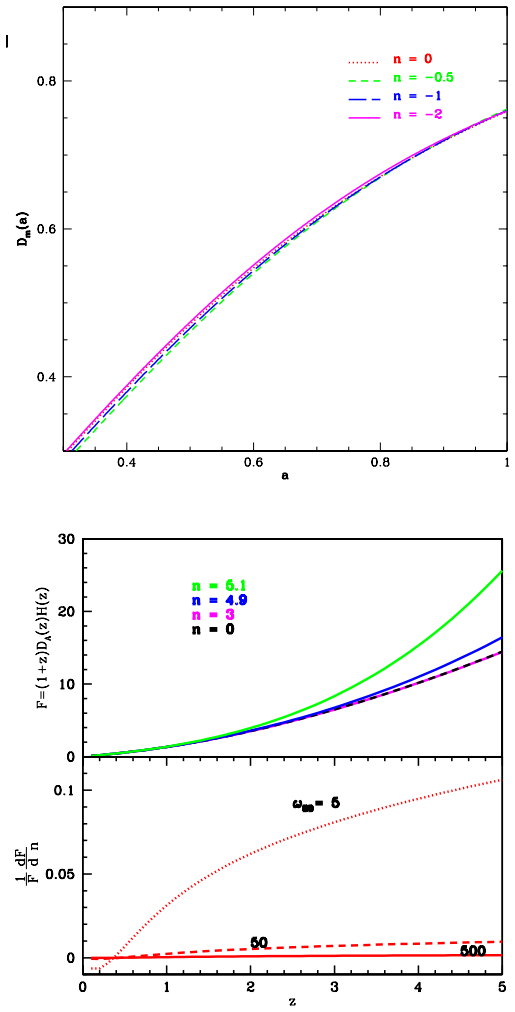

Figure 4. Top: The growth of matter for various values of n. Even when $m = 10$ is not too large, relatively small negative values of n help to approach GR. Bottom: The Alcock-Paczynski parameter for different values of the exponent n and $m = 100$. The sensitivity of APD to the exponent is almost absent today, however it increases as the redshifts increases as well, this tell us that high-redshift surveys are more capable of detecting a possible AP effect in BDT. Also Variation of the APD with respect to the exponent for different gBDT models. As we see if $m \to 1$ the sensitivity of APD to the exponent is larger. For the extreme case of $m = 5$ APD is detectable even at relatively low redshift.

On one hand, there is a damping of the anisotropies at small scales due to rescalings of G_N, since increasing the strength of gravity makes the visibility function wider it is more difficult for electrons to recombine. On the other hand, the size of the anisotropies estimated by the locations of the peaks is also affected due to modifications of the expansion history which give rise to different times of recombination.

In order to devail effects due to the variation of ω controled by the n parameter it is convienient to consider the following two regimes

1. **Large** m**.** For large m the model today is close to ΛCDM and then it is a viable model, if $n < 0$ the whole ω is large all along the expansion history and the visibility approaches to that of GR. Otherwise, when $n > 0$, the scalar is enhanced all along and so the expansion history is greatly modified unless m is sufficiently large to counter the effect.

2. **Small** m. In this case, unless the exponent is negative and large, the effects due to the scalar field are important. As expected the exponent only helps to approach the ΛCDM limit, as a result the visibility is sensitive only to the overall value of ω. However, even for small values of $n > 0$ the visibility departs in great extent from ΛCDM then they are very likely to be rejected by data as preferred models.

The following Table shows the values of ω at the time of recombination for relevant values of m and n within rEST models. Notice that even for small m, ω at recombination gets considerably large for relatively small values of $n < 0$.

$\omega(\tau_{rec})$			
	$m = 10$	$m = 100$	$m = 1000$
$n = 0.1$	4.96	49.7	496.9
$n = 0$	10	100	1000
$n = -0.5$	330.5	3301.7	33013.8
$n = -1$	1×10^4	1×10^5	1×10^6

The top panel of **Figure 3** shows that restricted and unrestricted models with $\phi_{in1} = 1$ and $n < 0$ tend to be indistinguishable for large values of m. On the contrary, even for small values of positive n

the visibility of both types of models differs significantly. In practice, if we aim to test the theory, such feature is useful since we suspect that the negative n are likely to be preferred by data because the average of ω along time is pushed to the ΛCDM limit if $n < 0$ for a given m. Nevertheless, the recombination history of rEST and uEST are too different for small $\omega(\tau_{rec})$ since they have different expansion rates. Regarding the rEST models, since $\omega(\tau_{rec})$ gets large if $n < 0$, the rescaling factor $(2\omega+4)/(2\omega+3)$ of the Newton constant easily tends to 1 at early times. Otherwise, if $n > 0$ then $(2\omega+4)/(2\omega+3) > 1$ hence the rEST model would have weaker Newton's constant than uEST, so it would reach the time of recombination before giving rise to a slightly narrower visibility function than in uEST.

Another observable quantity that responds to the EST parameters is the acoustic scale, Depending on the value of m, the extent of sensitivity of θ to n changes. The larger m is the lesser θ changes when n is varied as shown in the following Table.

$\theta(\tau_{rec})$		
n	$m = 1000$	$m = 10^6$
1	0.933639	1.035941
0.1	1.032737	1.037637
0.0	1.034614	1.037319
-0.3	1.036291	1.037173
-0.5	1.036713	1.036639

These results make clear that the measurement of the acoustic scale by the CMB could provide a good measurement of n and m. Although the location of the first peak remains unchanged when n varies (see **Figure 3**), the peaks at smaller scales suffer a further shifting which may provide a good measurement of θ.

Late ISW effect affecting photons travelling from the last scattering surface due to well potentials of galaxies formed at late times is considerably modified in EST models. Another source of ISW are the possible temporal variation of the potentials at late times. The former effect is manifested in the monopole of the temperature perturbation of the photon. **Figure 5** shows the ISW contribution to the temperature anisotropy in the line of sight integration for various EST models. For sufficiently large $n > 0$ the ISW gets enhanced and the scale at which it takes its maximum remains unaffected. In turn for $n < 0$ the spectrum is lowered and it takes its maximum on smaller angular scales. The BDT case ($n = 0$) differs considerably from the ΛCDM limit model, this tell us about a signature of BDT models and their close cousins with $n < 0$ imprinted in the ISW.

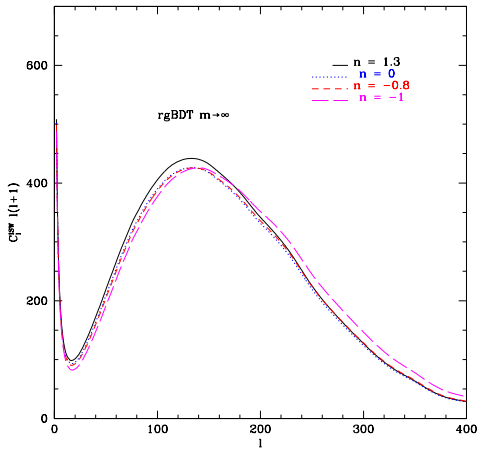

Figure 5. Effect of the EST parameters on the late ISW contribution to the temperature spectrum. For negative values of n the ISW spectrum shifts with respect of $n = 0$ due to different expansion histories while for positive n the ISW is enhanced.

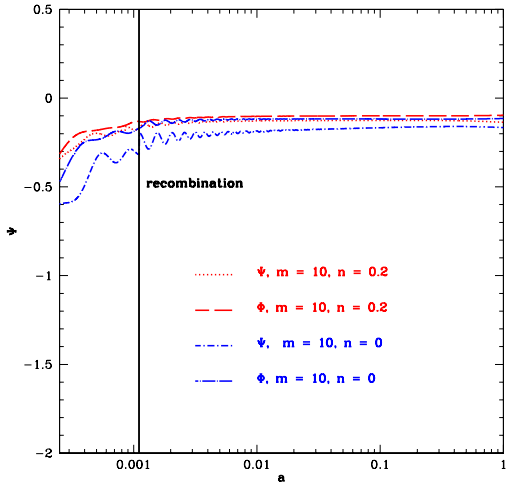

Figure 6. The gravitational potential Ψ within the EST for fixed m at the scale corresponding to the first peak in the temperature CMB spectrum. Acoustic driving also affects the third peak for positive n owing to these time-varying modes of the potentials.

The local time variation of ω carries much wealthier phenomenology in contrast to the BDT.

In the latter, the shape of the temperature and Doppler components of the spectrum is not significantly altered when constant ω is varied. In turn the shape of the components of the temprature spectrum is dramatically altered. When $n > 0$, on one hand, the spectrum stays within its 10% at scales larger than $l = 400$. On the other hand, for $500 < l < 1000$ the spectrum is boosted upwards (more significantly in the second and third peaks). At smaller scales $l > 1500$ the spectrum is not particularly sensitive to n. For $n <\sim 0$ the predominant effect is due to damping oscillations, however a special signature can be spotted in the first two peaks of both the monopole and Doppler spectra. When $|n|$ takes a more extreme value, the first two peaks get greatly enhanced whilst the next ones get importantly damped. This effect at large scales may be happening due to a combination of the ISW effect, Silk damping and acoustic driving. It is interesting that, in this last case, the CMB looks like one without CDM.

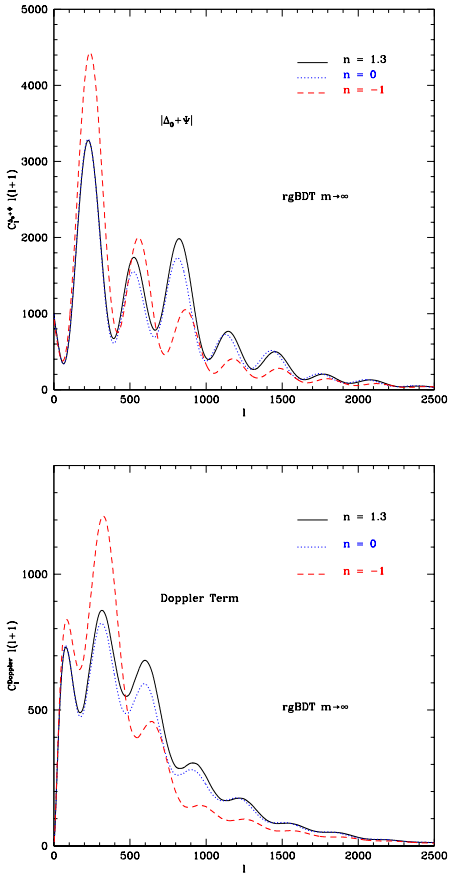

Figure 7. Angular spectrum of the monopole and the Doppler terms of the effective temperature perturbation of photons in the limit $m \to \infty$.

In EST the potentials vary in time **Figure 6** at some relevant scales and lead to an acoustic driving manifested in an enhancement of the amplitude of some modes. For small ω_{rec}, the last scattering surface is not far from the radiation to matter equality and so there are modes for which the potentials are still time varying to some extend. We can spot in **Figure 7** that around the 3rd peak is boosted due to this effect.

Photons of the CMB diffuse through the baryon fluid as a random walk leading to Silk damping of their perturbation (Silk, 1968.). The average distance that a photon goes across dubed as "the diffusion lenght" is given by $\lambda_D \sim \frac{1}{\sqrt{n_e \sigma_T H^{-1}}}$. The effect of this photon diffusion is to wash out anisotropies with wavelengths smaller than λ_D. The following Table shows the values of the scale of damping k_D for different EST models.

k_D			
	$m = 10$	$m = 100$	$m = 1000$
$n = 0.1$	0.1834	0.1426	0.1385
$n = 0$	0.1698	0.1412	0.1384
$n = -0.5$	0.1457	0.1388	0.1381
$n = -1$	0.1408	0.1383	0.1381

The physics governing the effects on the Doppler term carried by the variation n can be understood easily. This term is the contribution due peculiar velocities of galaxies along the line-of-sight. Therefore, before recombination the velocity of matter is proportional to the dipole of the baryon-photon fluid whilst after decoupling the more matter the universe contains the larger is the Doppler effect since the velocity of matter increase as the density of matter does. Thus if decoupling happens right after the time of equality, the Doppler term gets enhanced. The following table displays the time of equality happens for different EST models. By using it along with **Figure 2**, we can understand how the Doppler term is affected by n: On one hand, if $n < 0$ the larger is $|n|$ the closer are the times when recombination and equality of matter happen. On the other hand, if $n > 0$ as it increases either recombination and equality happen earlier so the effect is less important in this case.

τ_{EQ}			
	$m = 10$	$m = 100$	$m = 1000$
$n = 0.1$	75.77	115.03	120.76
$n = 0$	87.96	117.25	120.99
$n = -0.5$	113.09	120.56	121.34
$n = -1$	118.34	121.13	121.36

4. Constraints On The Effective Scalar-Tensor Theory

Methodology and Analysis

In order to obtain accurate predictions from EST, we numerically solved the background and linearized equations for perturbations in Jordan frame presented. Since matter is minimally coupled to the metric, equations for different components of the matter-energy in the universe remain just like in GR. This feature ensures that the effective gravitational strength is correctly implemented in the code. We implemented the synchronous gauge equations for scalar modes in a modified version of the CAMB package (Lewis, Challinor, & Lasenby, 2000).

In order to carry out a Bayesian analysis of the EST we sample the parameters space using the MCMC implementation in cosmology. We generated multiple chains for various combinations of models and data sets by means of the Metropolis-Hasting algorithm. Our chains were long enough to pass different convergence diagnostics processed by the GetDist program. The convergence diagnostics that we used are mainly the Gelman and Rubin "R= variance of chain means/mean of chain variances" statistic for each parameter using the second half of each chain (Brooks & Gelman, 1998). Also the Raftery and Lewis convergence diagnostics were used (Raftery & Lewis, 1992).

The main datasets we used are from the Planck satellite(Ade et al., 2013), WMAP-9 (Komatsu et al., 2011), the South Pole Telescope (SPT) (Schaffer et al., 2011) and the Atacama Cosmology Telescope(ACT) (Dunkley et al., 2013) and BAO (Eisenstein et al., n.d.).

As usual, the chains were generated for both rEST and uEST models. In rEST models have 8 parameters, the m and n parameters and the cosmological parameters which are the dimensionless baryon and dark matter densities ω_b and ω_c respectively, the ratio of the angular diameter distance to the sound horizon at recombination θ, the reionization redshift z_{re}, the amplitude and spectral index of the primordial power spectrum A_s and n_s . The Hubble constant H_0 and the (dimensionless) cosmological constant density ω_Λ are derived parameters. The uEST models have one additional parameter which is the initial condition $\bar{\phi}_{ini}$. All the other parameters including foreground astronomical parameters, fast parameters, calibration and beam parameters remain the same as in the original code (Ade et al., 2013; Neal, 2005; Lewis, 2013).

We now turn to the issue of priors. For the cosmological parameters we assume the same priors as for ΛCDM since the two types of cosmological evolution are very similar. A prior on H_0 (HST) from the measurement of the angular diameter distance from SHOES (Riess et al., 2009) is also imposed for some chains. The priors for the EST parameters are flat on $\bar{\phi}_{ini}$, $\ln(m)$ and n. In order to determine the allowed ranges by the analysis made in the previous section we take regions where EST resembles to GR at first glance. We left a wide range around these central values where these parameters are allowed to vary

5. Results and Discussion

Let us first discuss the results for the restricted models, which contain m and n as additional parameters to ΛCDM. We already proved that restricted and unrestricted models behave similarly. Nevertheless we did sample the space of parameters and obtained estimations for the parameters of both models in order to infer this conclusion a posteriori.

As probed in the previous section, both EST parameters are degenerate since the change in the expansion history depends on the overall value of ω. The effective result is a shift of the peak locations and peak heights. In order to single out the effect over the perturbations, we distinguish two regimes at which the theory approximate ΛCDM. The first one is characterized by $m \sim 1$ and $n < 0$ and the other one consists of models with $m \to \infty$ and n taking any value. It is reasonable to expect that the second region is preferred since it corresponds to a very small correction to the growth

of LSS in the phenomenological setup of rEST. In this region, when n is varied two main effects arise: at large scales the temperature anisotropy is enhanced due to the ISW and at intermediate scales, there is also a combined effect due to acoustic driving and silk damping affecting intermediate scales which is manifested as a boost in the amplitude of the second and third peaks. Other peaks for higher multipoles feel this effect in less extent.

It turns out that using Planck + WMAP9(pol) alone is not enough, in such case even if the number of samples is huge, the posterior distributions fail to pass the convergence diagnostics within an acceptable level. This lead us to the conclusion that further data was needed to constrain the parameters space. In order to get better results, we added HST and BAO. However, as we will see in short, some remaining degeneracies are still present.

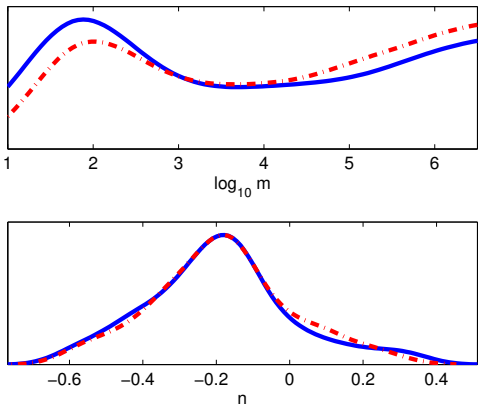

Figure 8. 1D marginal posterior distributions for uEST(red-dashed) and rEST(blue-solid) models with Planck+WMAP9(pol)+BAO+HST. Both sort of models have well defined regions of good likelihood: $m \sim 1$ and $m \to \infty$. According to Planck, the exponent n prefers small negative values which lead to a big overall value of ω along the expansion history.

According to the baseline set: Planck+ WMAP9(pol)+BAO+HST we can see that uEST and rEST 1D marginal posteriors have similar shape (see **Figure 8**). Notice that the high-likelihood regions that we foresaw in the previous section, clearly are picked by the data in both kind of models.

However we can spot a very small difference: uEST prefers the BDT region ($m \to \infty$) while the restricted models get on well with smaller m. This places rEST in an interesting place over uEST: if we keep in mind the indirect measure of modifications to the growth motivating the phenomenological setup of EST, it can be concluded that, according to combined measurements of the CMB by Planck and the expansion history by BAO and HST, a modification of the growth in GR is allowed and it would be of order $(1/m)$ today within 68% of confidence level. Thus, since smaller values of m lead to larger value of the modification to the growth, according to Planck, it is possible to detect deviations which are lesser suppressed in rEST than in uEST.

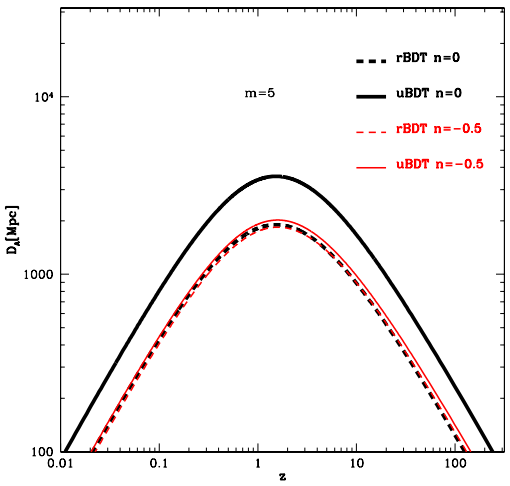

Figure 9. Angular diameter distance as function of the scale factor for different EST models.

Different preferred regions of uEST and rEST are closely related to the different sensitivities of the angular diameter distance to the n parameter of each type of model. **Figure 9** shows the predicted D_A in both types of models. A possible explanation would be that, once the CMB alone is fitted, the restricted case fits better the D_A measurements from BAO and HST than the unrestricted one.

In order to have a better idea on the features and quality of the 2σ and 1σ estimations for the EST parameters, lets have a look to their 2D marginal posteriors. The first outstanding characteristic is a considerable correlation between m and n. At 2σ such the well-constrained direction is well determined, however at 1σ two disconnected constraints arise at different degeneracy directions.

Above $m > 10^4$, the extent of correlation is the

same as for 2σ, in turn for $10 < m < 10^3$ the 1σ region(mild orange) bends in complicated way leading to a large correlation between the parameters. From projecting the l.h.s region of the 1σ constraint on vertical axis gives us an estimate for n (table 1). Notice that at 2σ the upper bound moves to larger values due to the leaning shape of the constraint.

Constraints of n with
Planck+WMAP9(pol)+HST+BAO

CL	mean	lower	upper
68	-0.47	-0.94	-0.15
95	""	-1.39	0.57
99	""	-1.45	0.84.

Results with Planck and other data different than WMAP(pol) give rise to very different constraints. Let us start from analyzing the 1D posteriors in **Figure 10** for the restricted model for the following datasets: Planck + WMAP9(pol) + High-l and Planck + lensing.

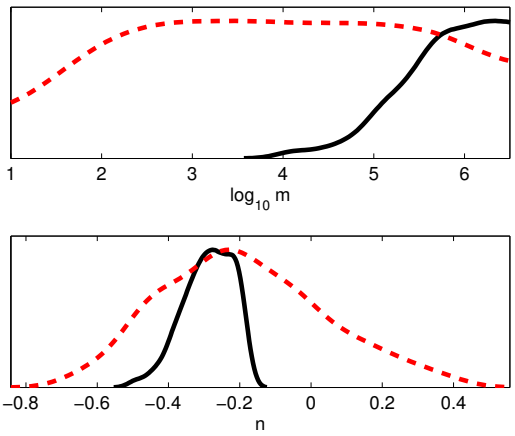

Figure 10. 1D posterior for m and n respectively within the restricted model with Planck + WMAP9(pol) + BAO + HST+ LENSING (red) and Planck + WMAP9(pol) + BAO + HST + ACT+SPT (black). Bottom: The inclusion of lensing gives rise to weak estimates of n whilst by adding the high-l data from ACT and SPT, the constraints become very strong. Top: the inclusion of lensing doesn't improve significantly the lower limit for m. Models with very large m, which were in principle expected to be close to ΛCDM, seem to be less likely than others with lower m; further analysis is needed in order to determine the reason why this happens. In contrast, when small-scales measurements are included, the lower limit of m is very well constrained.

As it happens small scales measurements of the CMB strongly constrain the EST parameters, the inclusion of high-l data dramatically changes the shape of the 1D marginal posteriors in comparison to Planck + WMAP9(pol). The well-spotted preferred low-high-m regions vanish for this dataset and the model gets strongly constrained, the lower limit of m is pushed up to the $m \to \infty$ limit while n firmly sticks to the $-1/2$ value and rejects positive values.

For Planck + lensing , the distribution shows us that a wide range of models with intermediate values of m are picked by the data and even though the exponent prefers negative values, $n < 1$ are not fully rejected as SPT does. It is interesting that lensing does not prefer the limit $m \to \infty$ as expected at first place. The fact that posteriors for Planck + WMAP9(pol) + SPT are tighter than for Planck + lensing tells us something about the extent of sensitivity of this datasets to the EST parameters.

6. Conclusion

The growth of LSS assumed in the phenomenological setup for modified theories of gravity considered here is assumed to behave as a power law $\mu = \mu_0(1 + ra^s)$. There is a correspondence between this setup and the effective scalar-tensor theory with $\omega(a) + 3/2 = m\, a^n$ where $m = 1/2r\mu_0$ and $n = -s$. We tested indirectly the free parameters involved using cosmological observations different to LSS. The main data set is the CMB anisotropies from Planck and tests of the expansion history from BAO and HST, that give rise to the 1σ constraint of $n = -0.47^{+0.32}_{-0.47}$ and two regions for m: $m = 50.1 \pm 11.2$ and $m > 3.2 \times 10^3$. The fact that the first of these regions is likely has an interesting consequence: according to the CMB, BAO and HST, the growth of LSS is allowed to hold a modification today of order $\sim 10^{-3}$ which is not negligible. Modifications of gravity within the Brans-Dicke family with running-ω along time are preferred by observations according to our results. Taking into consideration the degeneration of model to describe the background evolution (that is ignoring self-accelerated solutions) a host of Hordenski theories are compatible with our constraints as long their scalar field perturbation is approximated as that in the Brans-Dicke fam-

ily according to the mapping found in (Avilez & Skordis, 2014).

References

Ade, P. A. R., et al. (2013). Planck 2013 results. XV. CMB power spectra and likelihood. *A& A*, *571*, A15.

Alcock C., P. B. (1979). An evolution free test for non-zero cosmological constant. *Nature*, *281*, 358.

Avilez, A., & Skordis, C. (2014, Jul). Cosmological constraints on brans-dicke theory. *Phys. Rev. Lett.*, *113*, 011101. Retrieved from `http://link.aps.org/doi/10.1103/PhysRevLett.113.011101` doi: 10.1103/PhysRevLett.113.011101

Ballinger W.E., H. A., Peacock J.A. (1996). Measuring the cosmological constant with redshift surveys. *Mon. Not. Roy. Astron. Soc.*, *282*, 877.

Bergmann, P. (1968). Comments on the scalar-tensor theory. *Int. J. Theor. Phys.*, *1*(25).

Brans, C., & Dicke, R. H. (1961). Mach's principle and a relativistic theory of gravitation. *Phys. Rev.*, *124*, 925–935. doi: 10.1103/PhysRev.124.925

Brooks, S., & Gelman, A. (1998). Stephen brooks and andrew gelman. *Journal of Computational and Graphical Statistics*, *7*, 434-455.

Clifton, T., Ferreira, P. G., Padilla, A., & Skordis, C. (2012). Modified Gravity and Cosmology. *Phys.Rept.*, *513*, 1–189. doi: 10.1016/j.physrep.2012.01.001

Dodelson, S. (2003). *Modern cosmology*. Academic Press, Elsevier.

Dunkley, J., Calabrese, E., Sievers, J., Addison, G., Battaglia, N., et al. (2013). The Atacama Cosmology Telescope: likelihood for small-scale CMB data.

Eisenstein, D. J., et al. (n.d.). *Detection of the Baryon Acoustic Peak in the Large-Scale Correlation Function of SDSS Luminous Red Galaxies.* (submitted to the Astrophysical J., astro-ph/0501171)

Faraoni, V. (2009). Scalar field mass in generalized gravity. *Class.Quant.Grav.*, *26*, 145014.

Hojjati, A., Zhao, G.-B., Pogosian, L., Silvestri, A., Crittenden, R., & Koyama, K. (2012). Cosmological tests of general relativity: a principal component analysis. *Phys. Rev. D*, *85*, 043508.

Komatsu, E., et al. (2011). Seven-Year Wilkinson Microwave Anisotropy Probe (WMAP) Observations: Cosmological Interpretation. *Astrophys.J.Suppl.*, *192*, 18. doi: 10.1088/0067-0049/192/2/18

Lewis, A. (2013). Efficient sampling of fast and slow cosmological parameters. *Phys. Rev.*, *D87*, 103529. doi: 10.1103/PhysRevD.87,103529

Lewis, A., Challinor, A., & Lasenby, A. (2000). Efficient computation of CMB anisotropies in closed FRW models. *Astrophysical Journal*, *538*, 473-476.

L. Pogosian, K. K., A. Silvestri, & Zhao, G. B. (2010). How to optimally parametrize deviations from general relativity in the evolution of cosmological perturbations. *Phys. Rev. D*, *81*, 104023.

Matsubara T., S. Y. (1996). Cosmological redshift distortion of correlation functions as a probe of the density parameter and the cosmological constant. *Astrophysical Journal*, *470*, L1.

Neal, R. M. (2005, August). The short'cut metropolis method. *Technical Report*(0506).

Padmanabhan N., W. M. (2008). Constraining anisotropic baryon oscillations. *Phys. Rev. D.*, *77*, 3540.

Peebles, P. J. E. (1993). *Principles of Physical Cosmology.* doi: 10.1515/9780691206721

Raftery, A., & Lewis, S. (1992). How many iterations in the gibbs sampler? in bayesian statistics.

Riess, A. G., Macri, L., Casertano, S., Sosey, M., Lampeitl, H., Ferguson, H. C., ... Sarkar, D. (2009, July). A Redetermination of the Hubble Constant with the Hubble Space Telescope from a Differential Distance Ladder. *The AStrophysical Journal*, *699*(1), 539-563. doi: 10.1088/0004-637X/699/1/539

Schaffer, K., Crawford, T., Aird, K., Benson, B., Bleem, L., et al. (2011). The First Public Release of South Pole Telescope Data: Maps of a 95-square-degree Field from 2008 Observations. *Astrophys.J.*, *743*, 90.

Silk, J. (1968.). Cosmic black-body radiation and galaxy formation. *Astrophysical Journal*, *151*, 459.

Song, Y.-S., et al. (2010). Theoretical priors on modified growth parametrisations. *JCAP*, *1004*, 018.

Taruya A., N. T., Saito S. (2011). Forecasting the cosmological constraints with anisotropic baryon acoustic oscillations from multipole expansion. *Phys. Rev. D*, *83*, 3527.